Citation: Hirt, C., M. Rexer and S.Claessens (2015), Topographic evaluation of fifth-generation GOCE gravity field models – globally and regionally. In: Newton's Bulletin 5, Special issue on validation of GOCE gravity fields, accepted for publication.

Topographic evaluation of fifth-generation GOCE gravity field models – globally and regionally

Christian Hirt [1,2]
[1] Department of Spatial Sciences & The Institute for Geoscience Research, Curtin University, Perth, WA, Australia
[2] Institute for Astronomical and Physical Geodesy & Institute for Advanced Study, TU Munich, Germany
Email: c.hirt@curtin.edu.au

Moritz Rexer
Institute for Astronomical and Physical Geodesy & Institute for Advanced Study, TU Munich, Germany
Email: m.rexer@tum.de

Sten Claessens
Department of Spatial Sciences & The Institute for Geoscience Research, Curtin University, Perth, WA, Australia
Email: s.claessens@curtin.edu.au

Abstract

ESA (European Space Agency) has released a series of new-generation Earth gravity field models computed from gradiometry and GPS observations carried out aboard the GOCE (Gravity field and Ocean Circulation Explorer) satellite. In order to assess the quality of the new GOCE gravity fields, the sensitivity of satellite gravimetry to the gravitational attraction of the topographic masses can be exploited. This study uses topographic mass models to evaluate five generations of GOCE gravity models, both globally and regionally. As model representing Earth's topography, ice-sheet and water-body masses we use the new RET2014 rock-equivalent topography model by Curtin University (Perth). The gravitational potential of the RET2014 model is computed in spherical harmonics and in ellipsoidal approximation (ellipsoidal topographic potential, cf. Claessens and Hirt 2013, JGR Solid Earth, 118, 5991). We compare gravity from GOCE and from the RET2014 topography, whereby similar signal characteristics are taken as a sign of quality for the GOCE gravity fields. Our topographic evaluation shows a steadily improved agreement of the five model generations with topography-implied gravity, and increase in GOCE model resolution. For the fifth-generation GOCE gravity fields, full resolution is indicated to harmonic degree ~220 (90 km scales), and partially resolved gravity features are found to degree ~270 (time-wise approach, TIM) and degree ~290-300 (direct approach, DIR), As such, the 5th-generation GOCE models capture parts of the gravity field signal down to ~70 km spatial scales. This is a very significant improvement in satellite-only static gravity field knowledge compared to the pre-GOCE-era. Our comparisons show that models from the DIR approach improved relative to those from the TIM approach from the 2nd to the 5th generation, with DIR offering the best short-scale performance (from degree 240 and beyond). Considering the unprecedented gravity field resolution achieved, the GOCE gravity field mission performed beyond the expectations. The GOCE gravity fields will serve as a de-facto-standard in a range of applications encompassing geodesy, geophysics and oceanography.

Key words GOCE, gravity, topography, mass modelling, model evaluation

1. Introduction

Over a period of four years, European Space Agency (ESA)'s dedicated Gravity field and Ocean Circulation Explorer (GOCE) satellite mission has measured Earth's gravity field with unprecedented spatial resolution from space (e.g., van der Meijde et al. 2015). Launched in March 2009, the GOCE mission entered its operational phase in November 2009 and probed the gravity field till ~mid 2012 from a nearly circular orbit (altitude of ~255 km and inclination of 96.7°). Additional measurements were carried out during a low-flying mission phase at a lower altitude of ~255 to ~224 km (July 2012 to June 2013), and at ~224 km (June to October 2013).

The main instrument aboard the GOCE satellite was a satellite gradiometer for measurement of gravity gradients (second derivatives of the gravitational potential), complemented by GPS-based satellite-to-satellite tracking to enhance the gravity field recovery in the lower-frequency spectrum (Drinkwater et al. 2003, Rummel et al. 2011, Bock et al. 2014). ESA's GOCE-High-Level Processing Facility (HPF) was used to produce a series of spherical harmonic GOCE gravity field models using different data periods (first to fifth generation models), and processing strategies (e.g., Pail et al. 2011) known as time-wise approach (abbreviated as TIM) and direct computation approach (DIR), cf. Section 2.

The spatial resolution of any gravity model from satellite observations is governed by Newton's law of gravitation implying attenuation of gravity signals with the square of the satellite height. Thus, a particularly important constituent of the GOCE gravity observation is the gravity effect of those masses which are closest to the satellite – the uppermost layers of the lithosphere and hydrosphere, notably the topography, ocean water and ice masses.

The sensitivity of satellite gravimetry for the gravitational attraction of the topographic masses (e.g., Mahkloof and Ilk 2008, Janák and Wild-Pfeiffer 2010, Grombein et al. 2011, Hirt et al. 2012, Novák and Tenzer 2013) can be exploited to assess the quality of GOCE gravity fields. Good agreement among gravity computed from Earth's topography and measured by GOCE – e.g., in terms of signal correlation – is a quality indicator for the satellite model. This particularly holds at shorter spatial scales where the gravity field becomes strongly influenced by the topographic masses. Topographic evaluation techniques are often used to assess the quality of satellite-measured gravity fields of the terrestrial planets (e.g., Venus, Konopliv et al. 1999, Mars, Konopliv et al. 2011, and Moon, Lemoine et al. 2014), and were shown to be useful for gravity fields from the GOCE mission too (Hirt et al. 2012).

Over most areas of Earth, the global topography is known with much higher resolution than the resolution provided by the GOCE gravity models. Compared to model validation based on ground-truth observations (with often regionally limited coverage, see several other papers in this volume), topographic evaluation thus allows for a truly global feedback on GOCE from comparisons against the global topography. However, comparisons between GOCE and the topography can be done regionally too, which is useful e.g., over areas where ground-truth data is limited (e.g., Africa, South America or Antarctica), cf. Hirt et al. (2012).

Besides the model evaluation, there are further major areas of application where the topography is crucial for GOCE gravity applications. These include the computation of GOCE Bouguer gravity (e.g., Braitenberg 2013, Hirt 2014), and smoothing of GOCE gravity measurements (e.g., Janák and Wild-Pfeiffer 2010, Grombein et al. 2011, 2014). In both cases, gravity implied by the topography is subtracted from GOCE gravity in order to highlight effects associated with mass-density anomalies (Bouguer gravity), or to improve the quality of interpolation (smoothing). Topographic evaluation of

GOCE gravity fields, as done here, uses differences between gravity from GOCE and from the topography too, whereby a reduction in signal variability is taken as a sign of quality for the GOCE gravity fields.

This contribution focuses on the global and regional topographic evaluation of five GOCE model generations from the TIM and DIR approaches (Section 2). As model for the uppermost masses of the lithosphere and hydrosphere we use the newly developed RET2014 rock-equivalent topography model (http://ddfe.curtin.edu.au/models/Earth2014). This model represents the masses of Earth's topography, ice-sheets and water-bodies based on new or improved data sets (Section 3). The gravitational potential of the RET2014 model is computed using a recently developed gravity forward modelling technique (Claessens and Hirt 2013) that accounts for Earth's ellipsoidal shape (Section 4). It delivers the RET2014 gravitational potential in spherical harmonics and in ellipsoidal approximation, which is rigorously compatible with the mathematical representation of GOCE gravity field models.

In Section 5, gravity effects from the various GOCE models and from RET2014 are compared. This is done both in terms of cross-correlation, and signal reduction rates which quantify the amount of RET2014 gravity signals "observed" by GOCE. The comparisons are carried out as a function of the harmonic degree, and with geographic specificity over various regions (global, land, oceans, continents). This provides insight into (a) the spatial resolution of the GOCE models, (b) their sensitivity for short-scale gravity recovery, and (c) the relative performance of the DIR and TIM approaches over five model generations. Concluding remarks are given in Section 6.

Our paper builds upon the earlier study by Hirt et al. (2012) who evaluated the first three GOCE model generations using an initial version of Earth's RET (RET2011), and forward modelled gravity effects in spherical approximation (e.g., Rummel et al. 1988). Compared to our earlier study, recent progress includes (i) improved gravity forward modelling in ellipsoidal approximation, (ii) up-to-date mass modelling through RET2014, and (iii) inclusion of five GOCE model generations. In order to substantiate points (i) and (ii), earlier models of Earth's topographic potential are included in this study (cf. Section 3.2 and appendix A).

We acknowledge the many other studies concerned with evaluation of GOCE gravity field models using a range of complementary evaluation techniques, e.g., comparisons against ground gravity data (Gruber et al. 2011, Hirt et al. 2011, Voigt and Denker 2011, Tscherning and Arabelos 2011, Abdallah et al. 2012, Guimarães et al. 2012, Szucz 2012, Janák and Pitoňák 2011, Sprlák et al. 2011, 2012, Rexer et al. 2013, Gerlach et al. 2013, Godah et al. 2014), against global gravity models (e.g., Pail et al. 2011, Hirt et al. 2011), other satellite-collected data (Hashemi Farahani et al. 2013), and orbit comparisons (Gruber et al. 2011).

2. GOCE gravity models

ESA's GOCE satellite mission has triggered a new era of gravity observation from space. The reason for this advance is the sensitivity of GOCE's main gravity sensor (a gravity gradiometer) to signals at comparatively small spatial scales (up to ~ 80 km) w.r.t. to earlier satellite gravity missions such as GRACE (up to ~ 150 km) and CHAMP. Since the launch of the GOCE satellite a multitude of gravity field models incorporating GOCE gravity data have been published. Among the 26 listed models (http://icgem.gfz-potsdam.de/ICGEM/, accessed September 2014), the most important are ESA's official GOCE gravity field releases, which are based on three different processing approaches known as *direct* (DIR ; Bruinsma et al. 2010) , *space-wise* (SPW; Migliaccio et al. 2010) and *time-wise* (TIM; Pail et al. 2010) method. The models are the result of the joint effort of ESA's *High-Level Processing Facility* (HPF), involving ten European universities and research institutes under the management of

Technische Universität München. For the details and further literature on the different processing strategies we refer to Pail et al. (2011). The processing approaches follow different philosophies e.g. regarding outlier detection, stochastic modelling, constraining, a priori information and combination with other sources of gravity data (Table 1). Hence, the different models come with different features and the user should carefully consider the choice of model based on the intended application.

While the production of *space-wise* models has been abandoned after the release of the second model generation in 2011, five model generations exist from each of the two other processing approaches (DIR and TIM). The fifth generation models, released in mid-2014, are the final versions of ESA GOCE models, as they incorporate the data of the entire operational mission time (November 2009 - October 2013), cf. Table 1. Detailed descriptions of the fifth-generation models are given in Bruinsma et al. (2014) for DIR5 and in Brockmann et al. (2014) for TIM5.

The previous generation models (1st to 4th) may be regarded as intermediate models because of two reasons: (a) they incorporate only a certain period of GOCE observations and (b) the processing strategies have been improved and were adapted to the mission's circumstances in course of time. An overview over the processing changes from the 1st to the 4th generation DIR and TIM models is given in Rexer et al. (2013). The processing details for each release can be found in the respective model header information and the additional data sheet (the latter has been released continuously from the 3rd generation onwards). The 5th generation models incorporate 14 additional months of GOCE observations w.r.t. to the 4th generation models. The maximum degree and order has been increased from 260 to 300 (DIR) and 250 to 280 (TIM). The DIR5 processing has been subject to two major changes:

(1) the Kaula regularization in DIR5 now already starts from degree 180, whereas this constraint was applied beyond 200 in DIR4;

(2) the low harmonic degrees (up to degree 130) in DIR5 (apart from SLR contributions) now rely entirely on the ten years GRACE (release 3) normal equations of GRGS / CNES (Bruinsma et al. 2009). The GFZ GRACE release 05 (Dahle et al. 2012), present in DIR4 between degree 55 and 180, has been taken out.

In contrast to the rigorous GOCE-only gravity models of the TIM group, DIR models shall yield excellent performance over the entire spectrum. This is because they are full combinations of GOCE-SGG (beyond degree 130), GRACE (Tapley and Reigber 2001) and LAGEOS (Tapley et al. 1993). The latter two missions provide global gravity data of superior accuracy in the long wavelengths and are therefore highly complementary to the GOCE sensors. The TIM models rely on GOCE's GPS-SST (satellite-to-satellite) tracking data only in the lower frequencies, which cannot 'compete' with GRACE's Ka-band measurements. Therefore the TIM5 model, similar to the previous TIM releases, shows higher formal errors in the lower harmonic bands compared to DIR5. In the processing strategy of TIM5 two changes can be found:

(1) an increased harmonic degree of the GPS-SST normal equations based on the short-arc integral approach (now 150 compared to 130 in TIM4);

(2) the coefficients are now subject to Kaula regularization beyond degree 200 (previously beyond degree 180).

However, the largest difference between the 5th and the 4th generation models is not related to the nature of the processing strategies but in the orbit lowering of the GOCE satellite, commenced in late 2012. In its extended mission phase GOCE has been incrementally manoeuvred to an orbit altitude of

224 km (reached in June 2013) until the satellite's deorbiting in October 2013. The orbit lowering resulted in higher sensitivity for short-scale gravity signals, as the gravity attenuation effect is mitigated (Bruinsma et al. 2013; Schack et al. 2014). Therefore (and because of additional data in general), both 5th release models show significantly lower errors in the high harmonic degrees as well as higher spherical harmonic resolutions. The evolution of the models from the 1st generation to the 5th generation shows a continuous improvement w.r.t to the respective predecessor model, e.g., in terms of cumulative geoid errors (Fig. 1), which are derived from the formal errors of the models' coefficients. Note that the magnitude of the formal error estimates of DIR releases (as provided along with the models in terms of the coefficients' standard deviation) tend to be too optimistic in general (pers. comm. Sean Bruinsma and Roland Pail). The observed magnitude of DIR errors (from external validation) is rather in the order of TIM formal error estimates (Rexer et al. 2013).

Table 1. Main characteristics of all five model generations of the time-wise (TIM) and the direct (DIR) method; GRACE: Gravity Recovery And Climate Experiment; SLR: Satellite Laser Ranging; GRGS: Groupes de Recherches de Géodésie Spatiale; CNES: Centre National d'Etudes; GFZ: GeoForschungszentrum Potsdam; SGG: Satellite Gravity Gradiometer; SST: Satellite-to-Satellite Tracking; DIR : GO_CONS_GCF_2_DIR (1,2,3,4,5) ; TIM : GO_CONS_GCF_2_TIM (1,2,3,4,5).

	Release date	Model acronym	Data period	Effective data [months]	Lmax	Auxilliary data used [years]	Release specific comment	Model specific comment
R1	2010	DIR1	2009/11/1 - 2010/01/11	2	240	EIGEN5C	-	Combined solution making use of terrestrial data at short scales
		TIM1	2009/11/1 - 2010/01/11	2	224	none		pure GOCE-only solution
R2	2011	DIR2	2009/11/1 - 2010/06/30	8	240	ITG-GRACE2010s	-	SGG: band pass filter 10-125 mHz GOCE-SST up to 130 Exclusion of terrestrial data
		TIM2	2009/11/1 - 2010/07/05	8	250	none		processing strategy unchanged w.r.t. previous release-
R3	2011	DIR3	2009/11/1 - 2011/04/19	11.5	240	GRACE: 6.5 SLR: 6.5	-	GRACE and SLR as normal equations
		TIM3	2009/11/1 - 2011/04/17	12	250	none		SGG: inclusion of V_{xz}-compo5nent
R4	2013	DIR4	2009/11/1 - 2012/08/01	28	260	GRACE: 9 SLR: 25	Increased accuracy on all scales due to new Level-1b processing (Stummer et al. 2012)	SGG: inclusion of V_{xz}-component GRACE: GRGS/CNES and GFZ solutions
		TIM4	2009/11/1 - 2012/06/19	26.5	250	none		SST: short-arc integral method up to 130 (Mayer-Gürr et al. 2006)
R5	2014	DIR5	2009/11/1 - 2013/10/20	42	300	GRACE: 10 SLR: 25	Increased accuracy and spatial resolution due to orbit lowering.	GRACE : only GRGS/CNES Kaula: starting at 180
		TIM5	2009/11/1 - 2013/10/20	42	280	none		SST: up to 150 Kaula: starting at 200

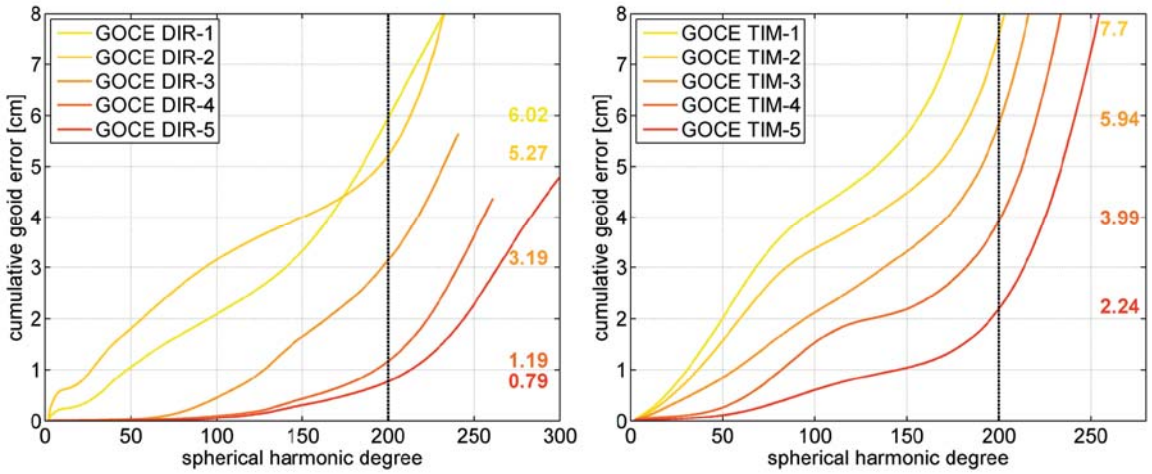

Fig. 1. Cumulative geoid height error of all generations of GOCE models of the direct (left) and the time-wise (right) approach with the numerical values of the error at degree 200 (= intersection of model with black dashed line) ; DIR: GO_CONS_GCF_2_DIR (1,2,3,4,5) ; TIM: GO_CONS_GCF_2_TIM (1,2,3,4,5).

3. Rock-equivalent topography (RET) and mass modelling

3.1 The new RET2014 model

To describe the masses of Earth's visible topography, ocean water, lake water and ice masses based on the newest data sets, the RET2014 model was developed as part of Curtin University's Earth2014 suite of global Earth topography models (Hirt and Rexer 2015). RET2014 is a composite model that represents ice and water masses as mass-equivalent layers of rock. RET2014 uses

(i) The 250m (7.5 arc-sec) release of the SRTM V4.1 topography (Jarvis et al. 2008) over land areas between +-60° latitude,

(ii) the 2014 version 9 release of the SRTM30_PLUS (Becker et al. 2009) bathymetry model over the oceans (30 arc-sec resolution)

(iii) Bedmap2 (Fretwell et al. 2013) bedrock, bathymetry and ice thickness data over Antarctica (1 km resolution) and

(iv) The 1km-resolution Greenland_Bedrock_Topography_V3 (GBT_V3) product (J.L. Bamber 2014, pers. comm., Bamber et al. 2013) over Greenland,

see Hirt and Rexer (2015) for full details. The RET2014 model is publically available via http://ddfe.curtin.edu.au/models/Earth2014, allowing replication of our study. The procedures applied to generate the RET2014 topography are largely similar to those used for the predecessor models RET2012 and RET2011 (cf. Hirt 2013, Hirt et al. 2012). We computed RET heights H_{RET} from SRTM30_PLUS, Bedmap2 and GBT_V3 by compressing water and ice masses into RET using

$$H_{RET} = H_{BED} + \frac{\rho}{\rho_R}\Delta H \qquad (1)$$

where H_{BED} is the bedrock, lake bottom or seafloor height (reckoned negative if below the geoid), ΔH is the thickness of the ice or water body, ρ_R is the mass density of topographic rock, and ρ the mass density of the ice or water body (see Table 2 for density values used). Over ice-covered water bodies (e.g., ice shelves), ice and water are compressed and stacked via

$$H_{RET} = H_{BED} + \frac{\rho_W}{\rho_R}\Delta H_W + \frac{\rho_I}{\rho_R}\Delta H_I \,. \qquad (2)$$

Anywhere over dry land, the heights of the topography are identical with RET heights. A spherical harmonic series expansion of the RET2014 topography grid to degree and order 2,160 was generated following the procedures outlined in Hirt (2013).

Table 2. Mass-density values used in RET2014

Mass body	Symbol	Mass density [kg m^{-3}]
Topography	ρ_R	2670
Ocean water	ρ_O	1030
Lake water	ρ_L	1000
Ice water	ρ_I	917

We acknowledge that even today the geometric knowledge of water bodies (bathymetry) is incomplete over areas devoid of direct depth measurements (see Becker et al. 2009), this equally holds for the lower boundaries of the ice-sheets (bedrock) over areas where direct ice thickness measurements are absent or scarce (Fretwell et al. 2013). Further, all data sets used may be subject to artefacts (e.g., spikes, data or interpolation errors), which are mostly of high-frequency nature. At the spatial scales observed by GOCE (say 70 km and larger), these imperfections are assumed to be rather uncritical for the topographic evaluation of the GOCE gravity fields.

3.2 Previous versions of RET models

As previous versions of Earth's rock-equivalent topography, we include Curtin University's RET2011 model (Hirt et al. 2012), and RET2012 (Hirt 2013) which were used in earlier topographic evaluations of GOCE gravity fields. Both RET models are based on 'older' ice and bathymetry data compilations. RET2011 relies on the DTM2006.0 spherical harmonic model of Earth's topography and bathymetry (Pavlis et al. 2007), while RET2012 as direct predecessor of RET2014 uses topography and bathymetry from SRTM V4.1 and SRTM30_PLUS (version 7). Both predecessors use RET computed from ETOPO1 (Amante and Eakins 2009) ice and bedrock data over Antarctica and Greenland (the data of which is now superseded by Bedmap2 and GBT_V3). As further differences between the three versions

- water masses of the major inland lakes are modelled in RET2014 and RET2012 (but not RET2011),
- ice-covered water bodies are modelled in RET2014 (but not RET2011 and RET2012).
- the RET-compression over ice-covered land is partially erroneous in RET2011 and RET2012 where bedrock heights are below the geoid. The error in RET2011 and RET2012 affects those fraction of the ice-sheets below the geoid which was incorrectly compressed by a factor of $(1-\rho_I / \rho_R) \approx 0.65$ instead of $\rho_I / \rho_R \approx 0.35$. In RET2014, all ice masses (below and above the geoid) are compressed by ρ_I / ρ_R (Eqs. 1 and 2).

Table 3 summarises the data sets used to generate the three generations of RET models.

Table 3. Data sources and detail of modelling for three generations of RET models

Input data \ RET version	**RET2014 (This work)**	**RET2012**	**RET2011**
Land topography	SRTM V4.1[&]		SRTM ~2004-release[*]
Ocean bathymetry	SRTM30_PLUS v9	SRTM30_PLUS v7	Smith and Sandwell (~2004) bathymetry[*]
Inland bathymetry	SRTM30_PLUS v9	SRTM30_PLUS v7	Not modelled
Antarctica – surface	Bedmap2	Bedmap1[+]	
Antarctica – bedrock	Bedmap2	Bedmap1[+]	
Greenland – surface	GBT_V3	GLOBE topography[+]	
Greenland – bedrock	GBT_V3	NSDIC bedrock[+]	
RET-modelling: ice	ice-sheets, ice-shelves,	ice-sheets	
RET-modelling: water	oceans, major lakes, water below ice (shelves, lake Vostok)	oceans, major lakes	oceans

[&] artefacts detected and removed over Asia and other areas, as described in Hirt et al. (2014)

[*] as provided through the DTM2006.0 series expansion by Pavlis et al. (2007)

[+] as provided through the ETOPO1 topography model by Amante and Eakins (2009)

3.3 Role of isostatic compensation

It is well known that at large spatial scales (say ~100s to 1000s of km) the limited rigidity of the Earth's crust cannot mechanically support the load of the topographic masses (e.g., Watts 2011). This phenomenon leads to isostatic compensation of the topography, i.e., a thickening of the Earth's crust below major mountain ranges. While the scientific foundation of isostasy is well established (see Watts 2011), accurate and detailed modelling of the isostatic compensation masses is not straightforward. Simplistic compensation models based on hypotheses such as Airy-Heiskanen or Pratt-Hayford are capable of describing isostatic compensation effects in coarse approximation only (Göttl and Rummel 2009). Observation-based crustal models describing the geometry of the crust-mantle interface (Moho) do not reach much higher resolution than 1 degree (about 110 km) globally, with lower resolution or dependence on gravity inversion over areas devoid of seismic Moho observations (e.g., Crust 1.0, Laske et al. 2013). Hirt et al. (2012) tested a range of isostatic compensation models, however, without improving the agreement between GOCE gravity and those implied by the uncompensated topography. This supports findings of an earlier study by Tsoulis and Stary (2005) who pointed out that "*Neither the long- nor the short-wavelength parts of the observed gravity field spectrum can be adequately explained by any of the existing isostatic models*".

In the absence of the sufficiently detailed and accurate isostatic compensation models, Earth's topography is treated as uncompensated in this evaluation study. At the spatial scales which are of particular interest for the GOCE mission (say 100 km scales), surface topography should be in good approximation uncompensated "*beyond harmonic degree 200*" (Wieczorek 2007), suggesting that isostatic compensation is not too much of concern for our study.

While the main focus of our topographic evaluation study is not on isostatic compensation, we note that GOCE observations are now being used to improve crustal models (see e.g., van de Meijde et al. 2015 and Reguzzoni et al. 2013) through gravity inversion. However, using these new GOCE-dependent models to describe isostatic compensation masses for the purpose of GOCE evaluation is not considered useful because it would be a cyclic procedure.

4. Methods

4.1 Computation of gravity from topography

The effect of the rock-equivalent topography on the Earth's gravitational potential, i.e. the topographic potential, was modelled using the harmonic combination method (Claessens and Hirt 2013). This method applies forward modelling of the Earth's topographic potential in the spectral domain, and generates a set of spherical harmonic coefficients of the topographic potential. The major advantage of this method over earlier methods (e.g., Rummel et al. 1988) is that it does not rely on a spherical approximation of the Earth, but rigorously computes the gravitational potential generated by topography referenced to a geodetic reference ellipsoid. In the harmonic combination method, powers of the topographic heights are expanded into surface spherical harmonic series with coefficients $\bar{d}_{nm}^{(k)}$

$$\bar{d}_{nm}^{(k)} = \frac{1}{4\pi} \int_{\sigma} \left(\frac{d_\Sigma}{r_e}\right)^k \bar{Y}_{nm} d\,\sigma \tag{3}$$

where k is the power of the topography, σ is the unit sphere, d_Σ is the topographic height above the reference ellipsoid measured along the direction to the ellipsoid's origin, r_e is the ellipsoidal radius, and $\bar{Y}_{nm}$ is the fully normalised (4π-normalised) spherical harmonic function of degree n and order m. The integration in Eq. (3) is performed in a spherical coordinate frame, using geocentric co-latitude and longitude. Solid spherical harmonic coefficients of the topographic potential ($\bar{V}_{nm}^R$) are then computed from a summation over these surface spherical harmonic coefficients ($\bar{d}_{nm}^{(k)}$) of equal order m (Claessens and Hirt 2013)

$$\bar{V}_{nm}^R = \frac{4\pi\rho b^3}{M(2n+1)(n+3)} \left(\frac{b}{R}\right)^n \sum_{k=1}^{n+3} \binom{n+3}{k} \sum_{j=0}^{\infty} (-1)^j \binom{-\frac{n+3}{2}}{j} e^{2j} \sum_{i=-j}^{j} \bar{K}_{nm}^{2i,2j}\, \bar{d}_{n+2i,m}^{(k)} \tag{4}$$

where ρ is the mean density of the rock-equivalent topography (2670 kg m^{-3} used here), b and e are the semi-minor axis and first numerical eccentricity of the reference ellipsoid (GRS80 parameters used; Moritz 2000), M is the Earth's mass (5.9725810×10^{24} kg used), R is the reference radius of the solid spherical harmonic series (6378137 m used), and $\bar{K}_{nm}^{2i,2j}$ are fully normalised sinusoidal Legendre weight functions. The latter can be computed recursively (see Claessens 2005, 2006, or Claessens and Hirt 2013 for details).

In this study, the RET2014 model of rock-equivalent topography was used as input in the harmonic combination method. The resulting model of the topographic potential was named dV_ELL_RET2014. Like EGM2008 (Pavlis et al. 2012), this model has a maximum spherical harmonic degree of 2190, containing (incomplete) coefficients beyond degree and order 2160 that are vital for accurate evaluation of the topographic potential at high resolution (Claessens and Hirt 2013). In the computation, the summation over k was truncated at $k = 10$, and the summation over j was truncated at $j = 30$. Claessens and Hirt (2013) have shown this to be sufficient, as both series converge fairly rapidly.

The gravitational attraction due to the topographic masses (in short: *topographic gravity*) can easily be evaluated anywhere on or above the Earth's surface from a topographic potential model such as dV_ELL_RET2014. This can be done in ellipsoidal approximation (e.g. Claessens 2006, Barthelmes 2009) or in spherical approximation. Spherical approximation was used here as it is sufficiently accurate for the purpose of this study. In spherical approximation, the topographic gravity δg_{TOPO} is given by

$$\delta g_{TOPO}(r,\theta,\lambda) = \frac{GM}{r^2}\sum_{n=0}^{n_{max}}\left(\frac{R}{r}\right)^{n+1}(n+1)\sum_{m=-n}^{n}\bar{V}_{nm}^{R}\bar{Y}_{nm}(\theta,\lambda) \quad (5)$$

where GM is the geocentric gravitational constant of the Earth (GRS80 parameter used; Moritz 2000).

4.2 Methodology for GOCE model evaluation

Following Hirt et al. (2012), we evaluate the GOCE model generations by comparing synthesised gravity from (a) GOCE and (b) the dV_ELL_RET2014 topographic potential model that is based on the RET2014 topography. In all comparisons, gravity is computed in narrow spectral bands of 5 harmonic degrees (e.g., degrees 6 to 10, 11 to 15, … 296 to 300, or lower, depending on the GOCE model) in terms of regularly spaced geocentric latitude-longitude grids of 10 arc-min spatial resolution. The computation height is set to 10,000 m above the surface of the GRS80 reference ellipsoid. This places the computation points safely outside the topographic masses where the field is non-harmonic.

The level of agreement between GOCE gravity δg_{GOCE} and topographic gravity δg_{TOPO} is quantified using cross-correlation coefficients (CCs)

$$CC = \frac{\sum(\delta g_{GOCE} - \overline{\delta g}_{GOCE})\sum(\delta g_{TOPO} - \overline{\delta g}_{TOPO})}{\sqrt{\sum(\delta g_{GOCE} - \overline{\delta g}_{GOCE})^2\sum(\delta g_{TOPO} - \overline{\delta g}_{TOPO})^2}} \quad (6)$$

and (signal) reduction rates (RRs)

$$RR = 100\%\left(1 - \frac{RMS(\delta g_{TOPO} - \delta g_{GOCE})}{RMS(\delta g_{TOPO})}\right) \quad (7)$$

where the symbols $\overline{\delta g}_{GOCE}$ and $\overline{\delta g}_{TOPO}$ denote mean values and RMS is the root-mean-square operator. CCs and RRs are computed as a function of (i) the GOCE model, (ii) the spectral band, and (iii) selected regions (the seven continents, all land and ocean areas, and the globe, cf. Fig. 2). In all cases we exclude

- all computation points located North of 83.3° and South of -83.3° latitude (these are areas not directly observed by GOCE due to the satellite's orbit inclination), as well as
- all computation points over Antarctica where bedrock elevations and ice-thicknesses depend on GOCE (see Fretwell et al. 2013 and Fig. 2). This ensures independence between GOCE and topographic gravity in our comparisons.

The two criteria CCs and RRs have the following testing power (after Hirt et al. 2012, Hirt 2014): CCs quantify the similarity between GOCE and topographic gravity, with strong correlation (say CCs of 0.7 or more) indicating good quality of the GOCE gravity fields. Complementary to CCs, signal reduction rates RRs quantify the portion of topographic gravity that is explained by the GOCE gravity observation. RRs of ~30% or higher indicate "*substantial topographic gravity signals explained by the GOCE observation*" (Hirt 2014), while lower but positive RRs demonstrate that parts of the (uncompensated) topographic gravity signal is observed by GOCE. Negative RRs occur when the difference δg_{TOPO} minus δg_{GOCE} possesses higher RMS signal strength than δg_{TOPO} alone (cf. Eq. 7), indicating that GOCE and topographic gravity signals are largely unrelated.

Fig. 3 gives an example of δg_{TOPO}, δg_{GOCE} and the difference δg_{TOPO} minus δg_{GOCE} over the Himalayas in spectral band of degrees 201 to 205 for three selected GOCE-TIM model releases. The

correlation and notable signal reduction are clearly visible, demonstrating a significant amount of GOCE-captured topographic gravity signals.

Note that the presence of mass-density anomalies (with respect to the reference density of 2670 kg m^{-3}) and any kind of modelling deficiency or observation error in δg_{GOCE} and δg_{TOPO} prevent RRs from approaching the theoretical maximum of 100 % (i.e., the GOCE-observed gravity signal δg_{GOCE} would be identical with the forward-modelled signal δg_{TOPO}). In practice, RRs do not exceed ~50% over continental areas and ~65% over very mountainous regions at the spatial scales observed by GOCE. CCs are capable of indicating the agreement between gravity signal patterns (lows and highs) only, which however does not provide information on the agreement between gravity signal magnitudes. The latter information is delivered by RRs.

Based on practical experiences, CCs and RRs are not computed for individual harmonic degrees. This is because the presence of correlations among the GOCE SHCs – and among the topographic potential SHCs (because of the underlying harmonic combination method, see Claessens and Hirt 2013) – would lower the mutual agreement between GOCE and topographic gravity. Computation of CCs and RRs over narrow spectral bands (here 5 degree band-width) reduces this effect as well as oscillations in the CCs and RR curves across the spectrum. Using spectral bands of few harmonic degrees band-width is also common in other validation studies, e.g., Gruber et al. (2011).

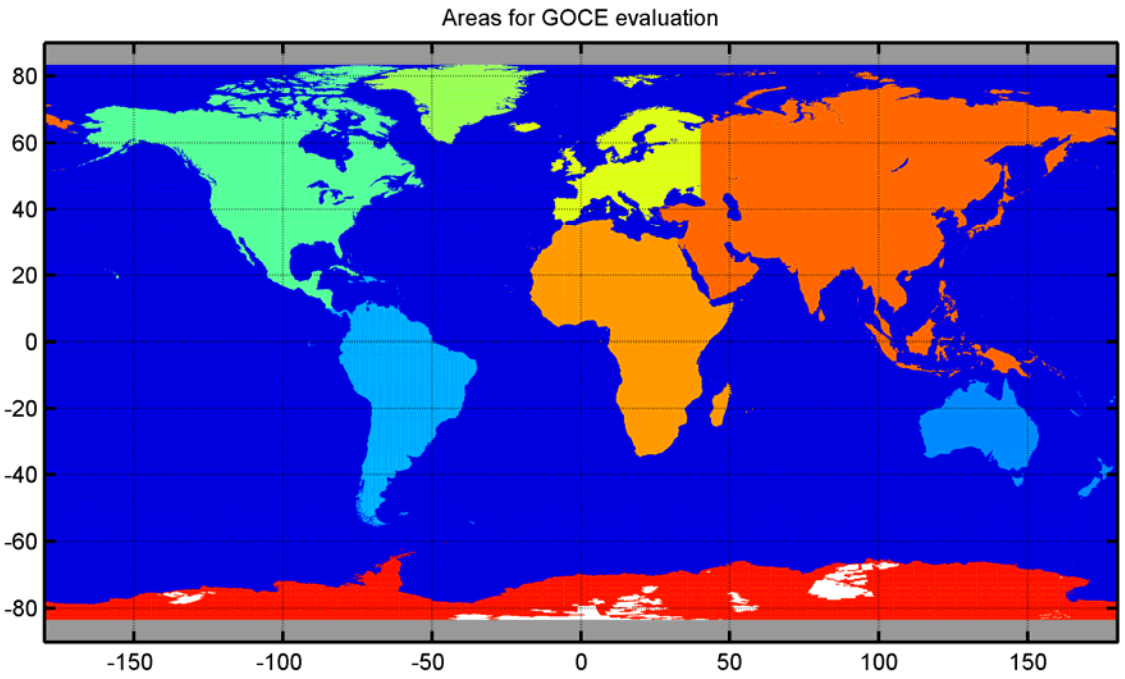

Fig. 2. Areas for evaluation of GOCE gravity field models. Oceans (dark blue), land/continental areas (various colours). Australia and New Zealand form the Oceania evaluation area. White areas over Antarctica indicate where Bedmap2 bedrock depends on earlier GOCE releases (excluded in all evaluations). Grey areas indicate the polar cap which is not directly observed by GOCE (excluded in all evaluations). Latitudes of this and all other maps are in terms of in geocentric coordinates.

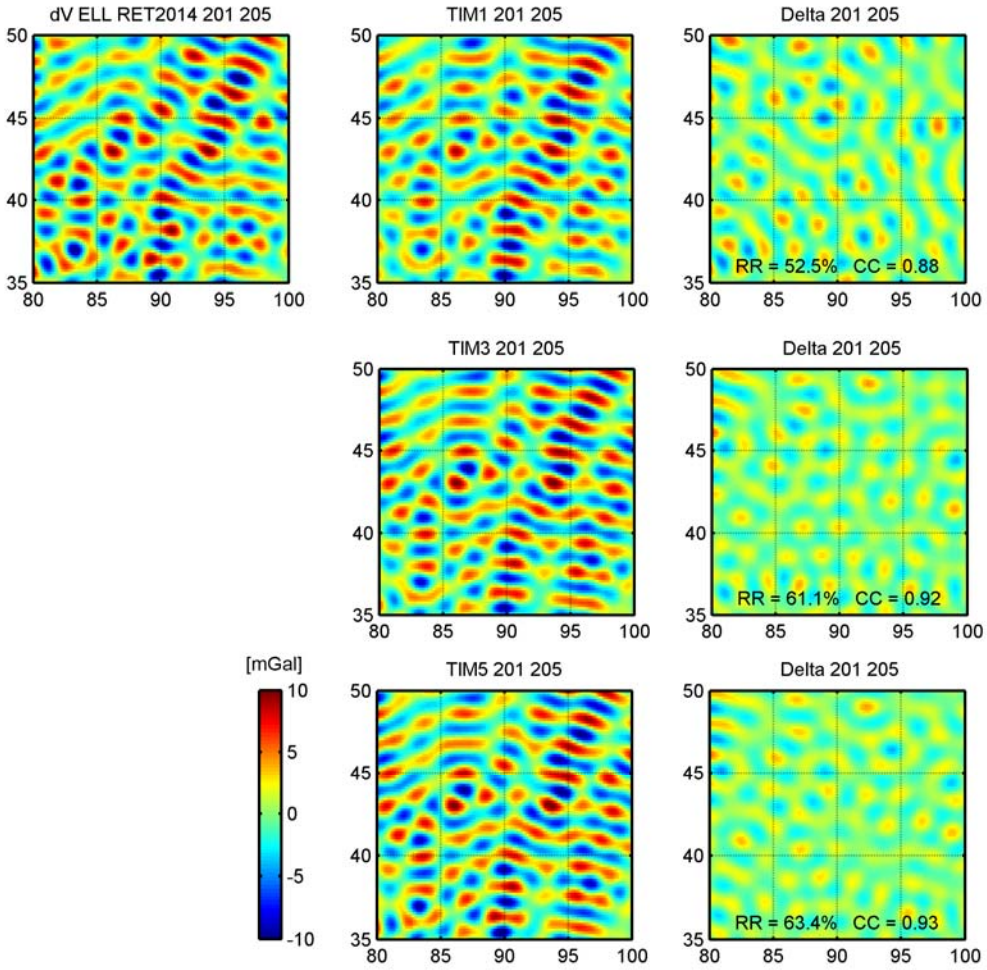

Fig. 3. Gravity effects implied by the RET2014 topography (left), and by GOCE TIM1, TIM3 and TIM5 models (middle column) in spectral band of degrees 201 to 205 over the Himalayas, differences between gravity from dV_ELL_RET2014 and GOCE (right column). Color range is ±10 mGal for all panels. The agreement between dV_ELL_RET2014 and GOCE gravity is very good, with CCs in excess of 0.9 and signal reduction (RRs) larger than 60% over the most rugged area of Earth. From top to bottom, the improved agreement from TIM1 to TIM5 is demonstrated. Residuals (right column) can be interpreted as a result of mass-density anomalies, and any kind of modelling/measurement errors in both data sets.

5. Results

5.1 Global comparisons

General observations

Fig. 4 shows CCs and RRs computed globally for the five GOCE model generations from the DIR and TIM approach. Fig. 5 provides the same indicators, however, separately for land and ocean areas. For all models, RRs steadily increase to 30-35% around harmonic degree 150, showing that the GOCE gravity observations explain a larger fraction of the gravity signal generated by the uncompensated topography as the harmonic degree increases. Depending on the model generation (2nd to 5th), and computation approach (TIM vs. DIR), all models experience a drop in RR, the 2nd generation around degree ~160-170, the 3rd near degree ~180, the 4th generation around degree ~190 and the 5th generation around degree 220 (seen in comparison to DIR1 which relies on terrestrial gravity data at short spatial scales). The drop in RR indicates that the respective model starts to “lose” the gravity signal, reflecting the effect of short-scale gravity signal attenuation at satellite height.

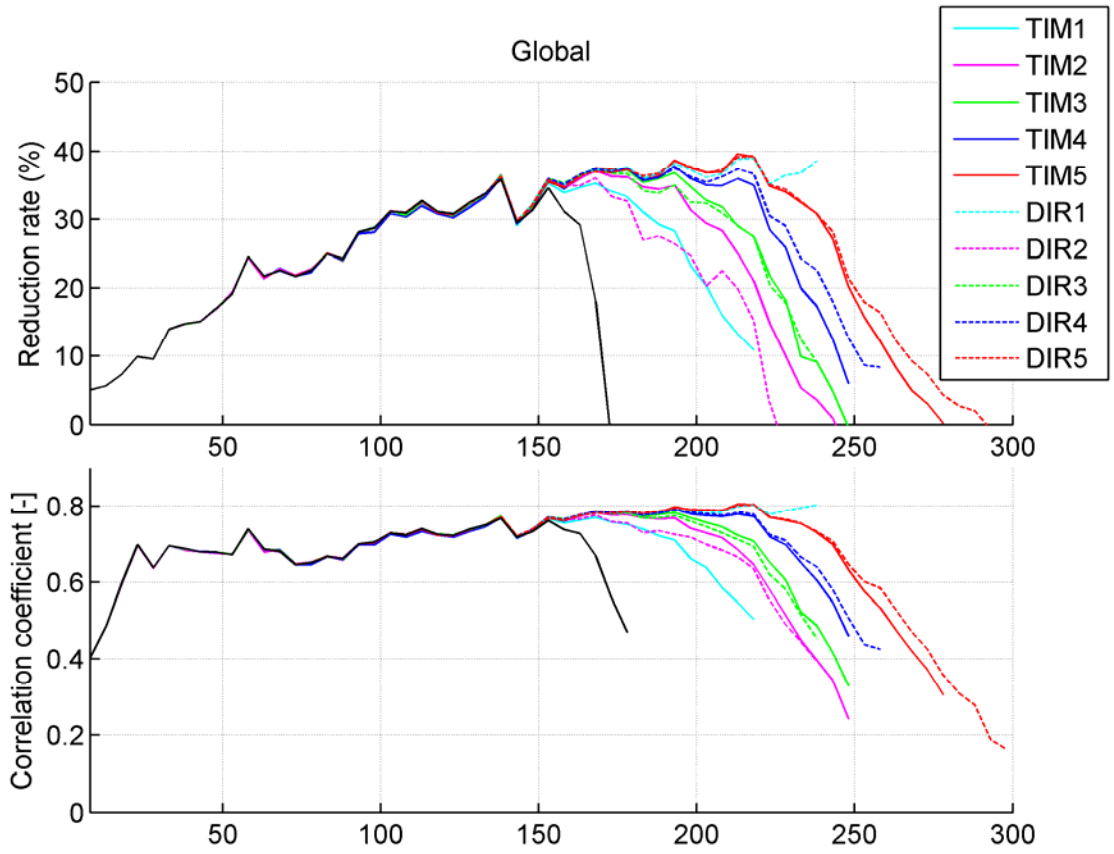

Fig. 4. RRs (top) and CCs (bottom) of 10 GOCE models and ITG-GRACE2010s (black curves) computed against dV_ELL_RET2014 near-globally (without polar regions and white areas shown in Fig 2). Indicators RR and CC are shown as a function of the harmonic degree (horizontal axes).

Notwithstanding, most of the models show positive RRs near or at their formal model resolution, showing that GOCE gravity captures topography-generated signals. Focussing on the 5th model generation which contains the 2012/2013 low-altitude observations, gravity from DIR5 (TIM5) reduces the RMS strengths of topographic gravity by ~10% at degree ~265 (~260), with RRs still being positive around degree ~275 (TIM5) and 285 (DIR5). This clearly demonstrates the presence of gravity signals at scales as short as ~70 km in the 5th-generation GOCE model releases, albeit in strongly attenuated form.

From Fig. 4 CCs are around +0.7 and larger over most of the spectrum, even at low degrees, and reach maximum values somewhat larger than +0.8 around degrees ~215-220 for the 5th generation GOCE releases. CCs start to drop around harmonic degrees ~160-170 (2nd), ~180 (3rd), ~200 (4th) and ~220 (5th generation), which reflects the increased quality of the GOCE models due to more observations, orbit lowering and improvements related to processing changes (see section 3). From a comparison between CCs and RRs, there is no one-to-one relation between both indicators. CCs are found to vary between +0.2 and +0.4 where RRs approach 0% in the high harmonic degrees. Conversely, for the low and medium harmonics, CCs are at the +0.7 level, while RRs show a steady increase (Fig. 4).

Comparison DIR vs. TIM

Both indicators allow discrimination between the short-scale performance of the DIR and TIM approaches for given model generations (Fig. 4). For the 2nd generation, TIM shows a better short-scale performance than DIR from degree 160 and higher, which is seen by RRs being up to 10%-points larger (e.g., around degree 200), likewise CCs being up to +0.05 larger. For the 3rd generation,

this behaviour is not so much pronounced anymore (RRs and CCs are close together, but with the indicators for TIM3 slightly better than for DIR3, also see results in Hirt et al. (2012). With the 4th model generation, there is a reversal in performance, with DIR4 offering the better short-scale agreement with topographic gravity: DIR4 is found to be around 3-5%-points (RRs) and 0.02-0.04 (CCs) above those of TIM4 beyond degree 200 (Fig. 4 and 5). For the 5th release, DIR5 and TIM5 offer a comparable performance against topographic gravity up to degree ~245-250. At very short spatial scales (70-80 km, or harmonic degrees 250 to 290), however, gravity from the DIR5 model offers better agreement with topographic gravity (5% advantage in terms of RRs, about 0.05 in terms of CCs). Holistically, these observations suggest performance improvements of the DIR-approach relative to the TIM-approach from the 2nd to 5th model generation.

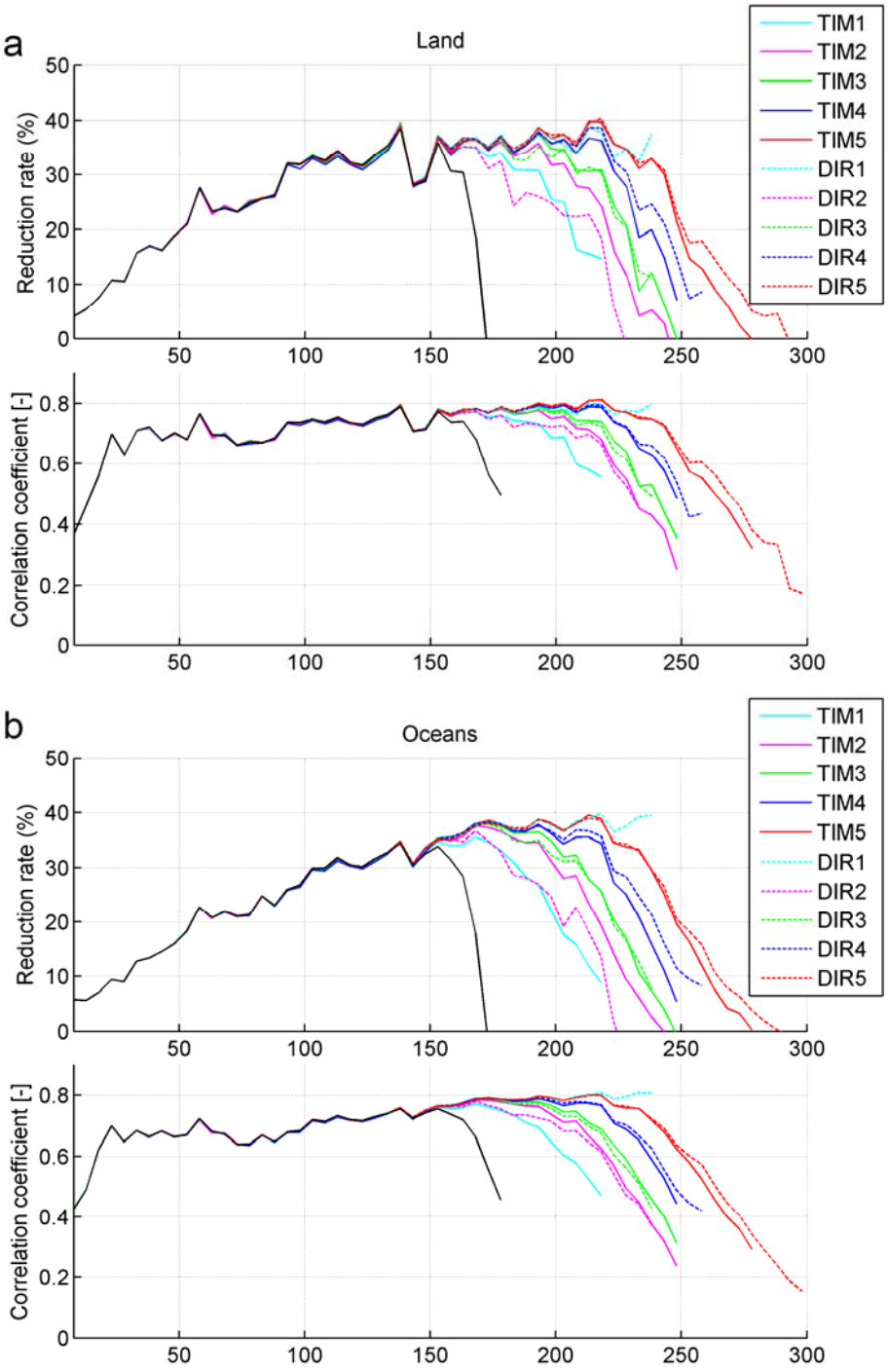

Fig. 5. As Fig. 4, but separate evaluations over the oceans (top panel), and land areas (bottom panel)

Comparison land vs. ocean

Fig. 5 essentially shows a comparable performance of the GOCE models over oceans and land areas (compare panel a with panel b), which suggests that the GOCE data quality is homogenous over land and oceans. The comparable performance also provides a feedback on the topographic gravity modelling, indicating similar quality of the RET2014 topography and dV_ELL_RET2014 topographic potential model over land and sea at the spatial scales observed by GOCE. RRs and CCs over land show somewhat more variability than over the oceans which is due to the smaller amount of computation points over land areas.

Comparison GOCE vs. GRACE

To demonstrate the steadily increased resolution of the GOCE gravity model generations, we have included the degree-180 ITG-GRACE2010s gravity model (Mayer-Gürr et al. 2010) as probably best satellite-only model of the pre-GOCE-era. From Fig. 4 and 5, ITG-GRACE2010s (black line) effectively resolves the gravity field to degree 160-165. Relative to the GRACE model, the 5th generation GOCE gravity fields provide new satellite-only gravity data to degree ~220-230, with some information up to degree ~300 (DIR5). The GOCE short-scale gravity signal recovery is exemplified for the DIR5-release in Fig. 6 over the Himalayas. The GOCE gravity mission thus improves gravity maps (w.r.t GRACE) in spectral band of degrees ~165 up to ~290, or at spatial scales of ~125 to ~70-80 km, which is a very significant addition to our gravity field knowledge from satellite-only data.

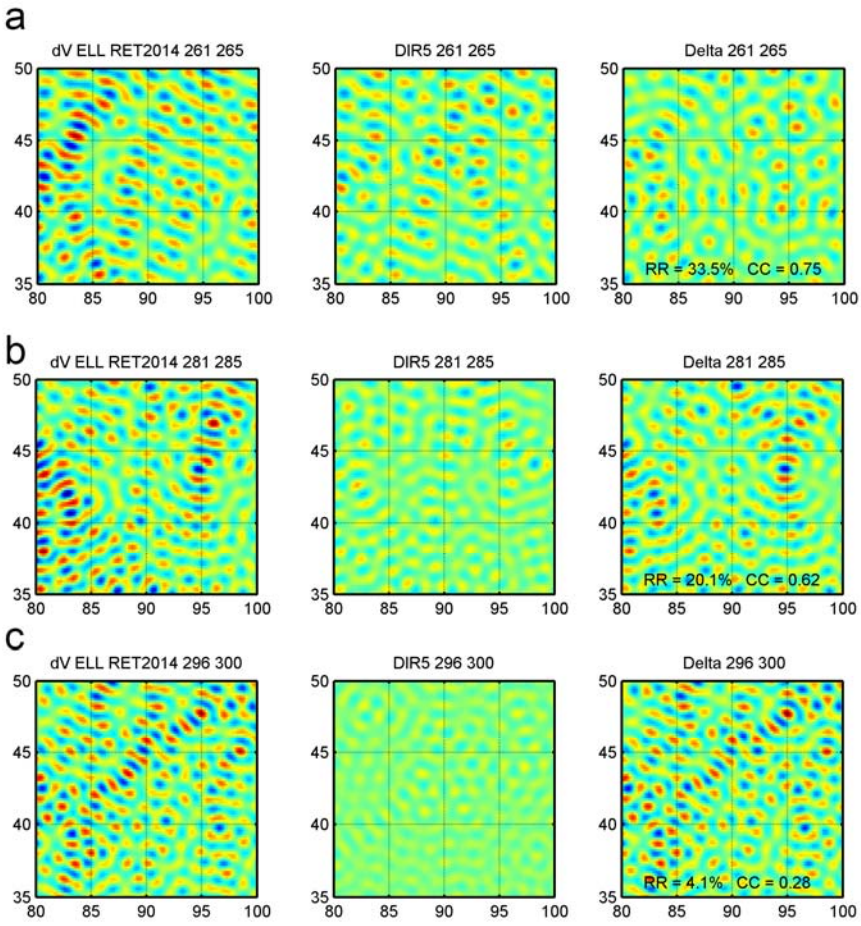

Fig. 6. Demonstration of DIR5 short-scale gravity signal capture over the Himalayas. Gravity from dV_ELL_RET2014 (left), gravity from DIR5 (middle), differences dV_ELL_RET2014 minus DIR5 gravity (right) in spectral bands 261 to 265 (a), 281-285 (b), and 296-300 (c). Color range is ±10 mGal for all panels. Note that subtraction of DIR5 gravity from dV_ELL_RET2014 gravity reduces RMS signal variability to some extent, even in spectral band 296-300 (by 4.1 %).

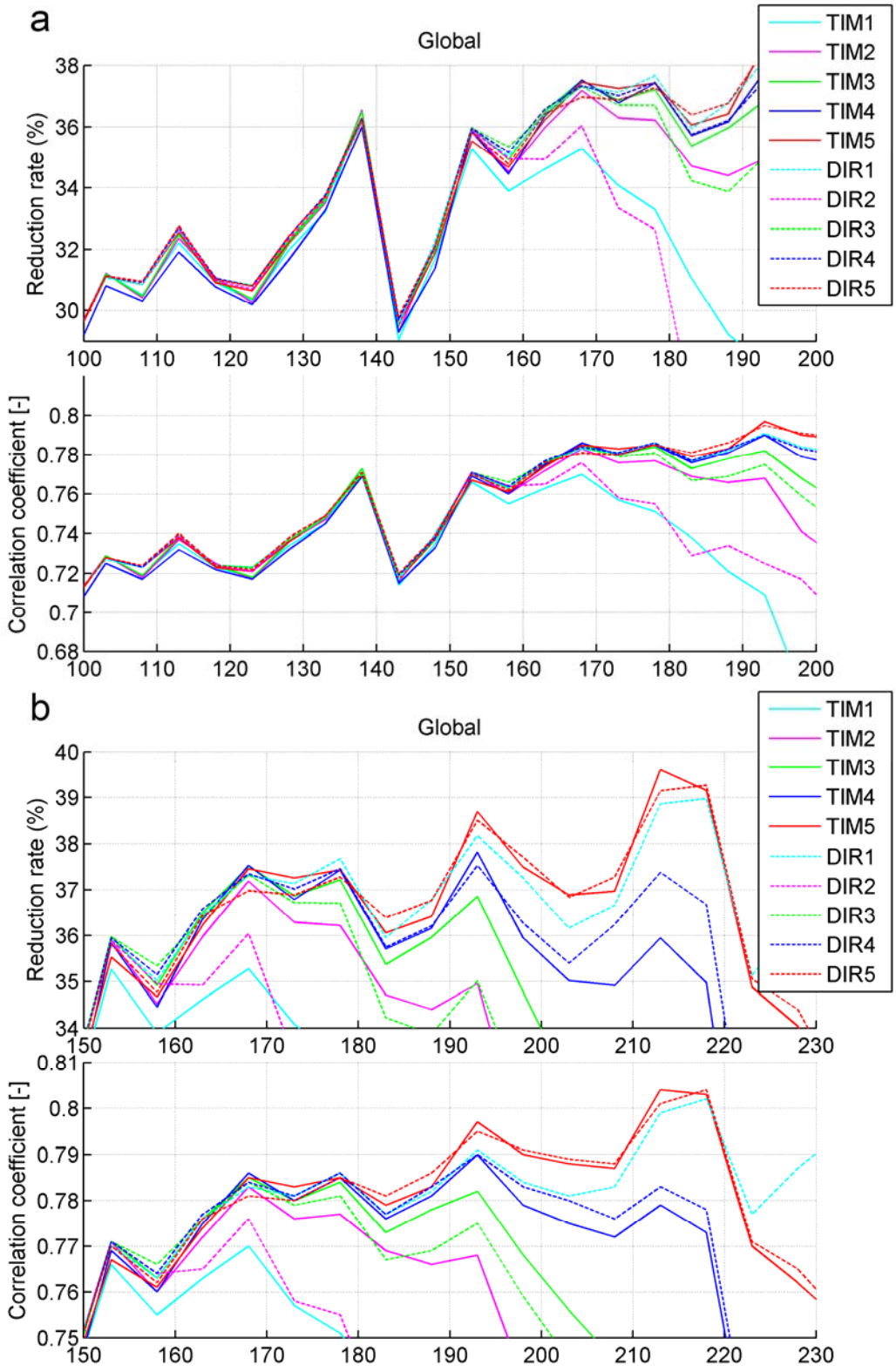

Fig. 7. As Fig. 4, but zoom into band of harmonic degrees 100 to 200 (a), and 150 to 250 (b). Note the behaviour of the 5th-generation models near degree 160. The RR and CC-agreement of the 5th-generation models DIR5 and TIM5 with the ground-gravity dependent DIR1-release (serving as a baseline) indicates full resolution of DIR5 and TIM5 to degree ~220.

Model performances in medium degrees

Fig. 7 shows the RRs and CCs over medium harmonic degrees (same data as in Fig. 4, but enlarged). From all models, the fifth model generation does not show the best performance over all harmonic degrees, despite incorporating the largest amount of GOCE observations from all models. This is evident in spectral window of degree ~150 to ~165, where DIR3, TIM3 and DIR4 offer higher RRs and CCs with respect to the RET topography. This somewhat unexpected observation could suggest a slight deterioration in quality of the 5th model generation over the predecessor models in the mid degrees. We also note that the TIM4 model shows lower RRs and CCs from degrees ~100 to ~170 compared to DIR4, TIM3 and DIR3, which is again not within the expectations, given the increased amount of data used in the 4th releases of the models. The interpretation of the above detected degradation of the 5th model generations w.r.t. previous generations within the band ~150 to ~165 is not easy, as there is a great variety of possible reasons to explain such a behaviour. Referring to the model and release specific comments in table 1, we may say that

- in case of TIM5 no obvious explanation for the degradation exists, as processing changes did not affect the band ranging from degree 150 to 180 (the same can be stated for the changes of TIM4 w.r.t TIM3)
- in case of DIR5, the change to the CNES/GRGS GRACE solution from degree 55 to 150 may explain for the behaviour in the affected band.

Note that the apparent degradation of the 5th model generations is very small (< 1% RR) in general and does not limit the usability of the latest models.

5.2 Regional comparisons

Fig. 8 and 9 show the two indicators over six continents (Europe, Asia, North/South America, Africa, Antarctica,), the Oceania region (Australia, New Zealand and surrounding islands), and Greenland as a continent-like land mass. In comparison to the indicator curves over global areas (Fig. 4 and 5), there are larger oscillations which reflect the effect of smaller numbers of data points over regional areas. For better legibility, the performance of the 2nd- 5th GOCE model generation are shown only.

The regional comparisons largely confirm the reported GOCE model characteristics, in that, the fifth generation models seem to fully capture gravity field features to degree ~220, while partially resolving the field to degree ~280. Over Africa, Oceania, and South America, DIR5 shows slightly positive RRs towards degree 300, demonstrating the recovery of topography signals at ~70km scales.

Over all of the regions, DIR5 and TIM5 show are mostly comparable performance to degree ~250, with somewhat higher RRs over Greenland, Oceania, Antarctica and Europe for DIR5. Beyond degree 250, a better short-scale performance is observed over most regions for DIR5. Depending on the region and spatial scale, RRs reach peak values between 40-48% around degree ~220 (Asia, North America, Europe, South America, Oceania), indicating a very significant portion of topographic gravity signals that is explained by 5th-generation GOCE gravity. As for the prior global investigations, in some regions the third generation models show slightly higher reduction rates than their successor models in the spectral band of degree 150 to 180 (see e.g. Greenland, North America and Asia).

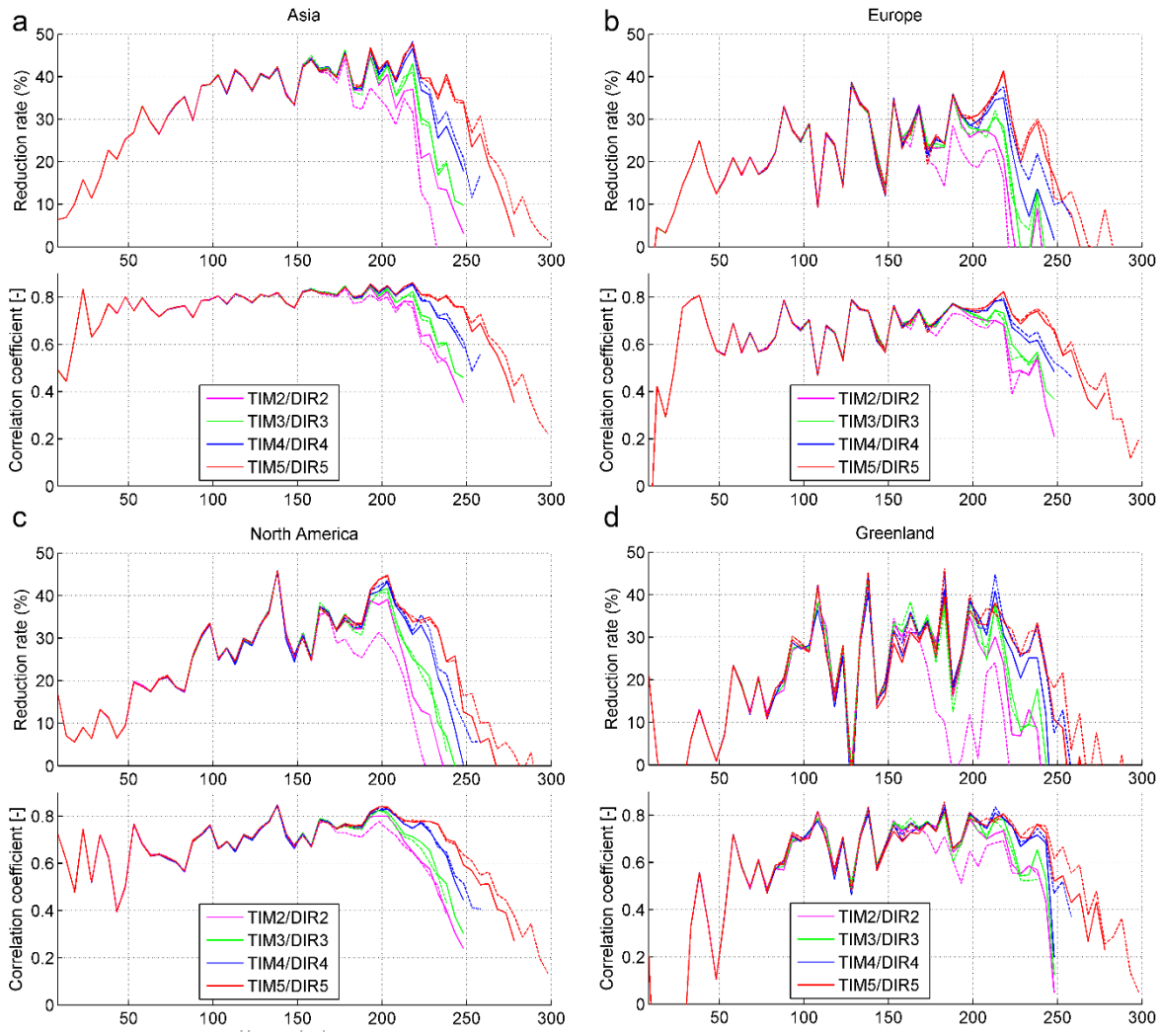

Fig. 8. GOCE evaluation results over the Northern Hemisphere continental areas. For better legibility, only the 2nd to 5th generation of DIR (dashed lines) and TIM (solid lines) approaches are shown.

6. Concluding remarks

The topographic evaluation technique was applied based on most recent topographic mass models and ellipsoidal gravity forward-modelling techniques to evaluate five generations of GOCE gravity field models from the DIR and TIM computation approach. The comparisons were performed over a range of narrow spectral bands using signal reduction rates and cross-correlation coefficients as key indicators. These indicate the level of agreement between gravity signal patterns and magnitudes from the topographic masses, and the GOCE mission. The topographic evaluation showed a steadily improved agreement of the five model generations with topography-implied gravity, and increase in GOCE model resolution.

For the fifth-generation GOCE gravity fields, our comparisons indicate full resolution of the DIR5 and TIM5 models to harmonic degree ~220 (90 km scales), and partially resolved gravity features to degree ~270 (TIM5) and degree ~290-300 (DIR5), with variations from these values over some of the continental areas tested. As such, the new GOCE models capture parts of the gravity field signal down to ~70 km spatial scales. This is a very significant improvement in satellite-only static gravity field data compared to the pre-GOCE-era, where the resolution of gravity from the GRACE mission was limited to about ~125km spatial scales (degree ~170).

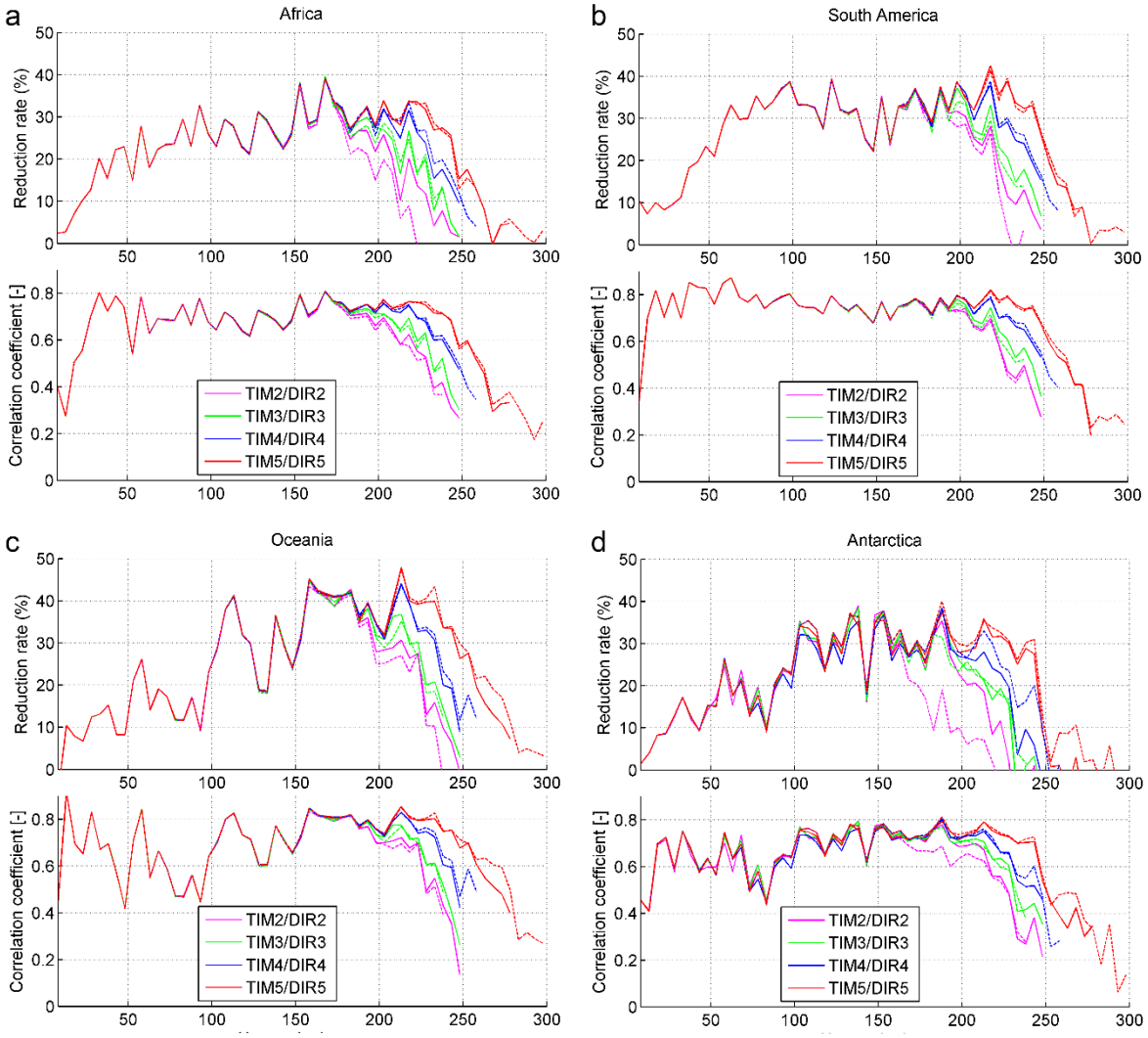

Fig. 9. GOCE evaluation results over the Southern Hemisphere continental areas. For better legibility, only the 2nd to 5th generation of DIR (dashed lines) and TIM (solid lines) approaches are shown.

Our comparisons showed that models from the DIR approach improved relative to those from the TIM approach from the 2nd to the 5th generation, with DIR5 offering the best short-scale performance (from degree 240 and beyond). At degrees less than 240, gravity from DIR5 and TIM5 is largely comparable.

Considering the unprecedented gravity field resolution achieved, the GOCE gravity field mission performed beyond the expectations. The GOCE gravity fields will continue to be used as a de-facto-standard in a range of applications encompassing geodesy, geophysics and oceanography.

Acknowledgements

We thank ESA and the GOCE model developers for making the GOCE gravity fields available to the community. Thanks are extended to the producers of digital elevation models used in this study. This work was supported by the Australian Research Council (ARC grant DP120102441), by Curtin University and by the Institute of Advanced Study (IAS), TU Munich through the German Excellence Science Initiative and the European Union Seventh Framework Programme under grant agreement 291763.

Appendix A

A1 Performance of various topography/ topographic potential models vs. GOCE

While the main scope of this paper is evaluation of the new GOCE gravity fields from latest topography, the evaluation technique can easily be 'reversed' by using GOCE gravity to provide feedback on different models of Earth's topographic masses and gravity computation techniques. We use DIR5 as the highest-resolution GOCE model (cf. Section 5) to provide the reference in these comparisons. Gravity is computed from a total of six topographic potential models developed over the past years and used in different gravity field studies. The input topography models are summarised in Table 3 and the derived topographic potential models in Table 4. These are the (i) dV_SPH_RET2011, and (ii) dV_SPH_RET2012 topographic potential models, which are both based on spherical approximation (i.e., use a mass-sphere as a reference, Rummel et al. 1988). The more recently developed (iii) dV_ELL_ETOPO1, (iv) dV_ELL_RET2012 and (v) dV_ELL_RET2014 topographic potential models rely on the more advanced ellipsoidal approximation (i.e., use of a mass-ellipsoid as a reference, Claessens and Hirt 2013).

Also included are the topographic potential coefficients of the (vi) Karlsruhe Institute for Technology (KIT)'s Rock-Water-ICE model (Grombein et al. 2011, 2014) abbreviated here to dV_KIT_RWI. In contrast to (i) to (v), the dV_KIT_RWI model does not use the concept of rock-equivalent topography, but instead models the potential of topography, ocean water, lake water and ice masses via volumetric layers *without* condensation. This approach is more accurate than the RET-compression, because the geometry of mass bodies is not changed. The dV_KIT_RWI model was developed through Newtonian integration in the space domain, followed by a subsequent harmonic analysis to obtain solid SHCs of the topographic potential. While models (i) to (v) are based on spectral-domain forward modelling, (vi) deploys forward modelling in the space domain. Fig. 10 shows the RRs and CCs of the six models computed against the GOCE DIR5 release. While the indicators do not sense notable differences in performance in the low harmonics (say to degree 50), the RR and CC curves start to diverge around degree 100. For the two spherically approximated models RRs are clearly lower than of all models in ellipsoidal approximation. This clearly shows that the ellipsoidal approximation level (iii-vi) is more compatible than the spherical approximation with GOCE gravity field models (reflecting that the actual mass distribution is more ellipsoidal than spherical), particularly in the higher harmonic degrees. This effect is not so pronounced in the CC-curves, but still visible (cf. Fig. 10).

The inter-comparison of the four ellipsoidal models reveals that the agreement between topographic and GOCE gravity becomes increasingly better with the incorporation of newer topographic data sets (compare dV_ELL_RET2012 with dV_ELL_RET2014). The highest RRs against GOCE DIR5 are observed for the new dV_ELL_RET2014 model, which particularly reflects the use of recent Bedmap2 data over Antarctica. CCs sense these improvements too, with the differences between the CC curves less pronounced than for RRs. The ETOPO1-based ellipsoidal topographic potential model shows RR and CCs comparable to those of dV_ELL_RET2012, which reflects similar data sources used in the model construction (cf. Table 3, differences are over the oceans and the SRTM releases over land).

RRs and CCs are mostly higher for the ETOPO1, RET2012 and RET2014-based ellipsoidal topographic potential models than for the dV_KIT_RWI model. This is most likely due to the use of newer data sets in RET2012 and RET2014 (KIT_RWI is based on the DTM2006.0 topography data base that include topography mass models available in or before 2006). It also suggests that the RET-compression in the dV_ELL_RET2012 and dV_ELL_RET2014 models little affects the RRs and CCs performance curves, so plays a minor role for the purpose of GOCE model evaluation. A detailed study on the role of the RET compression effect in topographic evaluation of satellite-observed

gravity fields would require the construction of "KIT-type" and RET-type" models from exactly the same data, which is not possible here, so remains as a future task. In summary, Fig. 10 shows the evolution of Curtin University's topographic mass modelling, with notable improvements through (a) the development and adoption of ellipsoidal forward modelling techniques, and (b) updates of the mass models through use of most recent topography data sets.

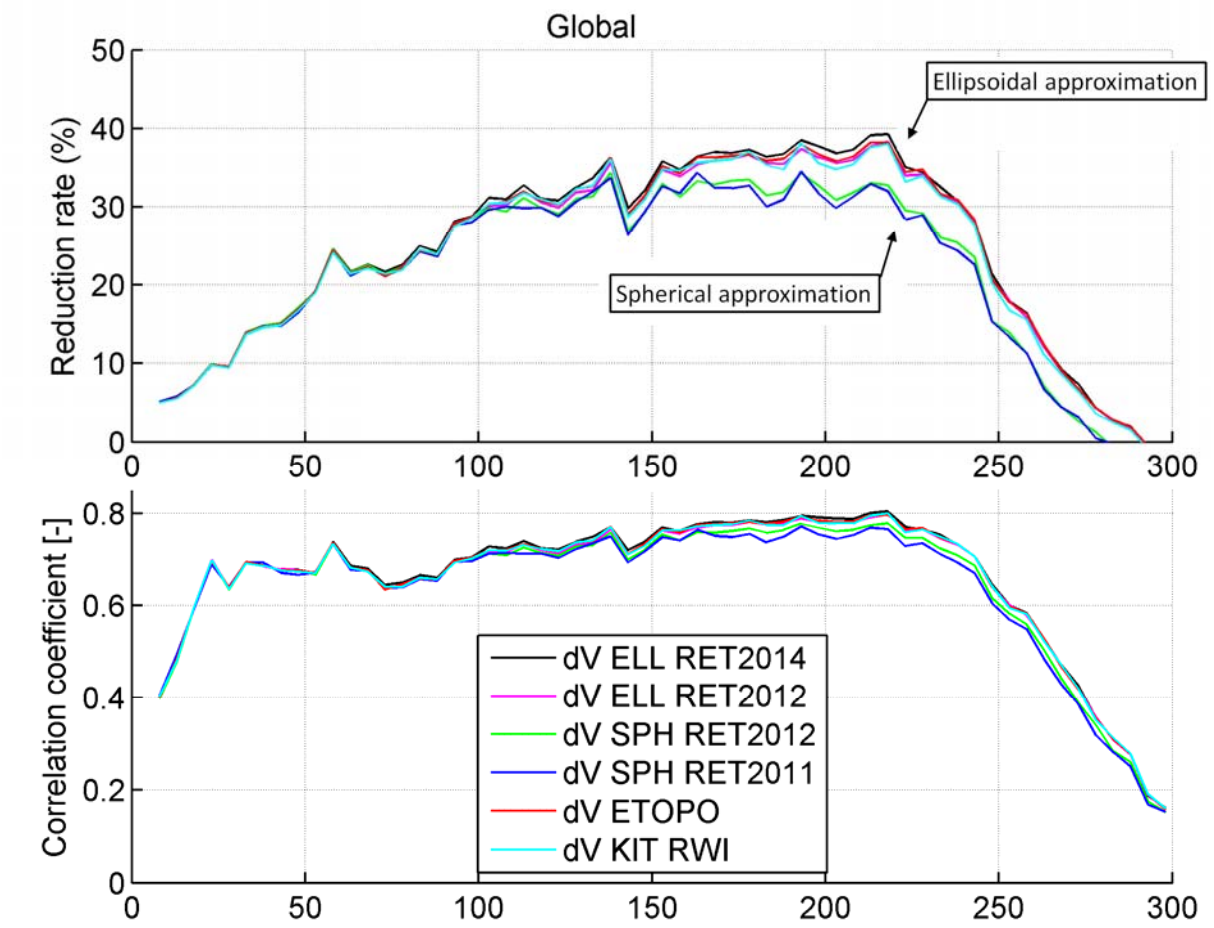

Fig. 10. Comparison of gravity from six topographic potential models against DIR5 over the near- global area (used in Fig. 6) in terms of signal reduction rates (top), and cross-correlation (bottom).
Gravity from all models was evaluated in terms of geocentric coordinate grids 10,000 m above the reference surface (sphere for models dV_SPH_RET2011/2012, and the GRS80 ellipsoid for the other models).

Table 4. Topographic potential models – input data and computation details

Potential model	Input-Topography	Level of approximation	Rock-equivalent topography (RET)	Reference
dV_SPH_RET2011	RET2011	Spherical	Yes	Hirt et al. 2012
dV_SPH_RET2012	RET2012	Spherical	Yes	Hirt & Kuhn 2012
dV_ELL_RET2012	RET2012	Ellipsoidal	Yes	Claessens& Hirt 2013
dV_ELL_RET2014	RET2014	Ellipsoidal	Yes	This work
dV_ETOPO1	ETOPO1	Ellipsoidal	Yes	Amante & Eakins 2009
dV_KIT_RWI	DTM2006	Ellipsoidal	No – direct modelling	Grombein et al. 2014

References

Abdalla, A., H. Fashir, A. Ali, and D. Fairhead (2012) Validation of recent GOCE/GRACE geopotential models over Khartoum state – Sudan, *Journal of Geodetic Science* 2:88–97, doi: 10.2478/v10156-011-0035-6.

Amante, C. and B. W. Eakins (2009), ETOPO1 1 Arc-Minute Global Relief Model: Procedures, Data Sources and Analysis. NOAA Technical Memorandum NESDIS NGDC-24, 19 pp, March 2009.

Bamber, J.L., J. A. Griggs, R. T. W. L. Hurkmans, J. A. Dowdeswell, S. P. Gogineni, I. Howat, J. Mouginot, J. Paden, S. Palmer, E. Rignot, and D. Steinhage (2013), A new bed elevation dataset for Greenland, *The Cryosphere*, 7, 499–510, doi:10.5194/tc-7-499-2013.

Barthelmes, F. (2009), Definition of Functionals of the Geopotential and their Calculation from Spherical Harmonic Models. Scientific Technical Report STR09/02, GeoForschungsZentrum Potsdam, Germany.

Becker, J.J., D.T. Sandwell, W.H.F. Smith, J. Braud, B. Binder, J. Depner, D. Fabre, J. Factor, S. Ingalls, S-H. Kim, R. Ladner, K. Marks, S. Nelson, A. Pharaoh, R. Trimmer, J. Von Rosenberg, G. Wallace and P. Weatherall (2009), Global Bathymetry and Elevation Data at 30 Arc Seconds Resolution: SRTM30_PLUS, *Marine Geodesy* 32(4): 355-371.

Bock, H., A. Jäggi, G. Beutler and U. Meyer (2014), GOCE: precise orbit determination for the entire mission, *Journal of Geodesy* 88(11), 1047-1060, doi: 10.1007/s00190-014-0742-8.

Braitenberg, C. (2013), Exploration of tectonic structures with GOCE in Africa and across-continents, *International Journal of Applied Earth Observation and Geoinformation* 35 (2015), 88–95, doi: 10.1016/j.jag.2014.01.013.

Brockmann, J.M., N. Zehentner, E. Höck, R. Pail, I. Loth, T. Mayer-Gürr and W.-D. Schuh (2014), EGM_TIM_RL05: An independent geoid with centimeter accuracy purely based on the GOCE mission, *Geophysical Research Letters* 41(22), 8089-8099, doi: 10.1002/2014GL061904.

Bruinsma S.L., J.M. Lemoine, R. Biancale, and N. Vales (2009), CNES/GRGS 10-day gravity field models (release 2) and their evaluation, *Adv. Space Res.* 45(4), 587-601, doi:10.1016/j.asr.2009.10.012.

Bruinsma S., J. Marty, G. Balmino, R. Biancale, C. Förste, O. Abrikosov, and H. Neumayer (2010), GOCE gravity field recovery by means of the direct numerical method. In: Lacoste-Francis H (ed) Proceedings of the ESA living planet symposium, 28 June–2 July, Bergen, ESA, Publication SP-686.

Bruinsma, S., J. Marty, C. Förste, O. Abrykosov, and S. Bonvalot (2013), Analysis of GOCE data after each orbit reduction - Abstracts, AGU 2013 Fall Meeting (San Francisco, USA 2013).

Bruinsma, S.L., C. Förste, O. Abrikosov, J.-M. Lemoine, J.-C. Marty, S. Mulet, M.-H. Rio and S. Bonvalot (2014), ESA's satellite-only gravity field model via the direct approach based on all GOCE data, *Geophysical Research Letters* 41(21), 7508-7514, doi: 10.1002/2014GL062045.

Claessens, S.J. (2005), New relations among associated Legendre functions and spherical harmonics, *Journal of Geodesy,* 79(6-7), 589 398-406, doi: 10.1007/s00190-005-0483-9.

Claessens, S.J. (2006), *Solutions to Ellipsoidal Boundary Value Problems for Gravity Field Modelling*, PhD thesis, Curtin University of Technology, Department of Spatial Sciences, Perth, Australia.

Claessens, S.J. and C. Hirt (2013), Ellipsoidal topographic potential – new solutions for spectral forward gravity modelling of topography with respect to a reference ellipsoid, *Journal of Geophysical Research - Solid Earth*, 118(11), 5991-6002, doi: 10.1002/2013JB010457.

Dahle, C., F. Flechtner, C. Gruber C, R. König, G. Michalak, and H. Neumayer (2012), GFZ GRACE Level-2 Processing Standards Document for Level-2 Product Release 0005, (Scientific Technical Report - Data , 12/02), Potsdam, 20 p, doi: 10.2312/GFZ.b103-1202-25.

Drinkwater, M.R., R. Floberghagen, R. Haagmans, D. Muzi, and A. Popescu (2003), GOCE: ESA's first Earth Explorer Core mission, In Earth Gravity Field from Space - from Sensors to Earth Sciences. In the Space Sciences Series of ISSI, Vol. 18, 419-432, Kluwer Academic Publishers, Dordrecht, Netherlands.

Fretwell, P., H.D. Pritchard, D.G. Vaughan, J.L. Bamber, et al. (2013), Bedmap2: improved ice bed, surface and thickness datasets for Antarctica, *The Cryosphere*, 7, 375-393, doi:10.5194/tc-7-375-2013, 2013.

Gerlach C., M. Šprlák, K. Bentel, B. Pettersen (2013), Observation, Validation, Modeling - Historical Lines and Recent Results in Norwegian Gravity Field Research, *Kart og Plan* 73(2):128 – 150.

Godah, W., M. Szelachowska, J. Krynski (2014), Accuracy assessment of GOCE-based geopotential models and their use for modelling the gravimetric quasigeoid – A case study for Poland, *Geodesy and Cartography* 63(1), 3-24, doi: 10.2478/geocart-2014-0001.

Göttl, F. and R. Rummel (2009), A Geodetic View on Isostatic Models, *Pure Appl. Geoph.*, 890 166(8-9), 1247-1260, doi: 10.1007/s00024-004-0489-x.

Grombein, T., K. Seitz, and B. Heck (2011), Smoothing GOCE gravity gradients by means of topographic-isostatic reductions, Proc. of '4th International GOCE User Workshop', Munich, Germany, 31 March – 1 April 2011 (ESA SP-696, July 2011).

Grombein, T., X. Luo, K. Seitz, and B. Heck (2014), A wavelet-based assessment of topographic-isostatic reductions for GOCE gravity gradients, *Surveys in Geophysics* 35(4), 959-982 doi: 10.1007/s10712-014-9283-1.

Gruber, T., P. Visser, C. Ackermann and M. Hosse (2011), Validation of GOCE gravity field models by means of orbit residuals and geoid comparisons, *Journal of Geodesy* 85(11):845–860, doi: 10.1007/s00190-011-0486-7.

Guimarães, G., A. Matos and D. Blitzkow (2012), An evaluation of recent GOCE geopotential models in Brazil, *Journal of Geodetic Science* 2:144–155, doi: 10.2478/v10156-011-0033-8.

Hashemi Farahani, H., P. Ditmar, R. Klees, J. Teixeria da Encarnacao, X. Liu, Q. Zhao and J. Guo (2013), Validation of static gravity field models using GRACE K-band ranging and GOCE gradiometry data, *Geophysical Journal International* 194:751–771, doi: 10.1093/gji/ggt149.

Hirt, C., T. Gruber and W. Featherstone (2011), Evaluation of the first GOCE static gravity field models using terrestrial gravity, vertical deflections and EGM2008 quasigeoid heights, *Journal of Geodesy* 85:723–740, doi: 10.1007/s00190-011-0482-y.

Hirt, C., M. Kuhn, W. Featherstone and F. Göttl (2012), Topographic/isostatic evaluation of new-generation GOCE gravity field models, *Journal of Geophysical Research - Solid Earth* 117(B05407), doi: 10.1029/2011JB008878.

Hirt, C. (2013), RTM gravity forward-modeling using topography/bathymetry data to improve high-degree global geopotential models in the coastal zone, *Marine Geodesy* 36(2):1-20, doi: 10.1080/01490419.2013.779334.

Hirt, C. (2014), GOCE's view below the ice of Antarctica: Satellite gravimetry confirms improvements in Bedmap2 bedrock knowledge, *Geophysical Research Letters*, 41(14), 5021-5028, doi: 10.1002/2014GL060636.

Hirt, C., M. Kuhn, S.J. Claessens, R. Pail, K. Seitz, and T. Gruber (2014), Study of the Earth's short-scale gravity field using the ERTM2160 gravity model, *Computers & Geosciences*, 73, 71-80, doi: 10.1016/j.cageo.2014.09.00.

Hirt, C. and M. Rexer (2015), Earth2014: 1 arc-min shape, topography, bedrock and ice-sheet models - available as gridded data and degree-10,800 spherical harmonics, *International Journal of Applied Earth Observation and Geoinformation* 39, 103-112, doi:10.1016/j.jag.2015.03.001. Available at: http://ddfe.curtin.edu.au/models/Earth2014.

Janák, J., and F. Wild-Pfeiffer (2010), Comparison of various topographic-isostatic effects in terms of smoothing gradiometric observations. In (Sansò, F. and Mertikas, S. P. P., ed), Gravity, Geoid and Earth Observation, International Association of Geodesy Symposia 135, 377-381, doi:10.1007/978-3-642-10634-7-50.

Janák, J. and M. Pitoňák (2011), Comparison and testing of GOCE global gravity models in Central Europe. *Journal of Geodetic Science* 1:333–347.

Jarvis, A., H.I. Reuter, A. Nelson, and E. Guevara (2008), Hole-filled SRTM for the globe Version 4, Available from the CGIAR-SXI SRTM 90m database. Available at: http://srtm.csi.cgiar.org.

Konopliv, A.S., W. B. Banerdt, and W. L. Sjogren (1999), Venus Gravity: 180th Degree and Order Model, Icarus 139, 3–18.

Konopliv, A.S., S.W. Asmar, W.M. Folkner, Ö. Karatekin, D.C. Nunes, S.E. Smrekar, C.F. Yoder and M.T. Zuber (2011), Mars high resolution gravity fields from MRO, Mars seasonal gravity, and other dynamical parameters, *Icarus*, 211, 401–428.

Laske, G., G. Masters, Z. Ma, and M. Pasyanos (2013), CRUST1.0 - A 1-degree Global Model of Earth's Crust,
Geophysical Research Abstracts Vol. 15, EGU2013-2658, EGU General Assembly 2013.

Lemoine, F.G., S. Goossens, T.J. Sabaka, J.B. Nicholas et al. (2014), GRGM900C: A degree-900 lunar gravity model from GRAIL primary and extended mission data, *Geophysical Research Letters*, 41(10), 3382-338, doi: 10.1002/2014GL060027.

Makhloof, A.A. and K.-H. Ilk (2008), Effects of topographic–isostatic masses on gravitational functionals at the Earth's surface and at airborne and satellite altitudes, *Journal of Geodesy* 82, 93-111, doi: 10.1007/s00190-007-0159-8.

Mayer-Gürr, T., A. Eicker, and K.-H. Ilk (2006), Gravity field recovery from GRACE-SST data of short arcs. In: Flury J, Rummel R, Reigber C, Rothacher M, Boedecker G, Schreiber U (eds) Observation of the Earth system from space. Springer, Berlin, pp 131–148.

Mayer-Gürr, T., E. Kurtenbach, and A. Eicker (2010), ITG-Grace2010 Gravity Field Model. URL: http://www.igg.uni-bonn.de/apmg/index.php?id=itg-grace2010, 2010.

Migliaccio F., M. Reguzzoni, F. Sanso, C.C. Tscherning and M. Veicherts (2010), GOCE data analysis: the space-wise approach and the first space-wise gravity field model; presented at the ESA Living Planet Symposium 2010, Bergen, June 27 - July 2, Bergen, Norway, 2010

Moritz, H. (2000), Geodetic Reference System 1980. *Journal of Geodesy* 74, 128-140.

Novák, P. and R. Tenzer (2013), Gravitational Gradients at Satellite Altitudes in Global Geophysical Studies, *Surveys in Geophysics* 34(5): 653-673, doi:10.1007/s10712-013-9243-1.

Pail, R., H. Goiginger, R. Mayrhofer, W.D. Schuh, J.M. Brockmann et al (2010), GOCE gravity field model derived from orbit and gradiometry data applying the Time-Wise Method. In: Lacoste-Francis H (ed) Proceedings of the ESA living planet symposium, 28 June–2 July, Bergen, ESA, Publication SP-686.

Pail, R., S. Bruinsma, F. Migliaccio, C. Förste, H. Goiginger, W.D. Schuh, E. Höck, M. Reguzzoni, J.M Brockmann, O. Abrikosov, M. Veicherts, T. Fecher, R. Mayrhofer, I. Krasbutter, F. Sanso and C.C. Tscherning (2011), First GOCE gravity field models derived by three different approaches, *Journal of Geodesy* 85(11):819–843, doi: 10.1007/s00190- 011-0467-x.

Pavlis, N.K., J.K. Factor, and S.A. Holmes (2007), Terrain-related gravimetric quantities computed for the next EGM. In: Proceed. of the 1st Intern. Symp. of the Intern. Gravity Field Service (IGFS), Istanbul, 318-323.

Pavlis N., S.A. Holmes, S. Kenyon, and J. Factor (2012), The development and evaluation of the Earth Gravitational Model 2008 (EGM2008). *Journal of Geophysical Research* 117, doi: 10.1029/2011JB008916.

Reguzzoni, M., D. Sampietro and F. Sansò (2013), Global Moho from the combination of the CRUST2.0 model and GOCE data, *Geophysical Journal International*, 195(1), 222-237, doi: 10.1093/gji/ggt247.

Rexer, M., C. Hirt, R. Pail, and S. Claessens (2013), Evaluation of the third- and fourth-generation GOCE Earth gravity field models with Australian terrestrial gravity data in spherical harmonics, *Journal of Geodesy* 88(4), 319-333, doi: 10.1007/s00190-013-0680-x.

Rummel, R., Rapp, R.H., Sünkel, H., Tscherning, C.C. (1988), Comparisons of global topographic/isostatic models to the Earth's observed gravity field. Report No 388, Dep. Geodetic Sci. Surv., Ohio State University, Columbus, Ohio.

Rummel, R., W. Yi, and C. Stummer (2011), GOCE gravitational gradiometry*, Journal of Geodesy* 85(11), 777-790, doi: 10.1007/s00190-011-0500-0.

Schack, P., C. Stummer, M. Rexer, R. Pail and T. Gruber (2014), Assessment of GOCE gradiometer data during low orbit mission phase; European Geosciences Union General Assembly, Wien, 01.05.2014.

Sprlák, M., C. Gerlach, O. Omang, B. Pettersen (2011), Comparison of GOCE derived satellite global gravity models with EGM2008, the OCTAS geoid and terrestrial gravity data: case study for Norway. In: Proceedings of the 4th International GOCE User Workshop, Munich, 31st March 2011, ESA SP-696, Noordwijk.

Sprlák, M., C. Gerlach and B. Pettersen (2012), Validation of GOCE global gravity field models using terrestrial gravity data in Norway, *Journal of Geodetic Science* 2(2):134–143.

Stummer, C., C. Siemes, R. Pail, B. Frommknecht, and R. Floberghagen (2012), Upgrade of the GOCE Level 1b gradiometer processor, *Advances in Space Research* 49(4):739–75, doi:10.1016/j.asr.2011.11.027.

Szucz, E. (2012), Validation of GOCE time-wise gravity field models using GPS-levelling, gravity, vertical deflections and gravity gradients in Hungary. *Civil Engineering* 56(1):3 – 11.

Tapley, B., and C. Reigber (2001), The GRACE mission: status and future plans. In: AGU Fall Meeting Abstr, Vol. 1.

Tapley, B., B. Schutz, R. Eanes, J. Ries, and M. Watkins (1993), LAGEOS laser ranging contributions to geodynamics, geodesy, and orbital dynamics, *Geodynamics Series* 24:147–173.

Tscherning, C.C. and D. Arabelos (2011), Gravity anomaly and gradient recovery from GOCE gradient data using LSC and comparisons with known ground data. In: Proceedings 4th International GOCE user workshop, Munich, ESA SP-696, Noordwijk.

Tsoulis, D. and B. Stary (2005), An isostatic compensated gravity model using spherical layer distributions, *Journal of Geodesy* 78(7-8), 418-424, doi: 10.1007/s00190-004-0404-3.

van der Meijde, M., R. Pail, R. Bingham and R. Floberghagen (2015), GOCE data, models, and applications: A review, *International Journal of Applied Earth Observation and Geoinformation*, Vol 35, Part A, March 2015, 4-15, doi: 10.1016/j.jag.2013.10.001.

Voigt, C. and H. Denker (2011), Validation of GOCE gravity field models by astrogeodetic vertical deflections in Germany. In: Proceedings of the 4th International GOCE User Workshop, SP-696, ESA/ESTEC, The Nederlands, vol 4.

Watts, A. B. (2011), Isostasy, In: Encyclopedia of Solid Earth Geophysics (Ed. Gupta, H. K.), 984 1, 647-662, Elsevier.

Wieczorek, M.A. (2007), The gravity and topography of the terrestrial planets. In: Spohn, T., 988 Schubert, G. (Eds.), *Treatise on Geophysics, vol. 10.* Elsevier-Pergamon, Oxford, 165-989 206.